

LINEAR ESTIMATION OF ELECTRON BERNSTEIN CURRENT DRIVE

J. M. GARCIA-REGAÑA,* F. CASTEJÓN, and A. CAPPA

Laboratorio Nacional de Fusión, EURATOM-CIEMAT, Madrid 28040, Spain

Received May 12, 2008

Accepted for Publication October 28, 2008

Electron Bernstein waves (EBWs) have been confirmed as a suitable choice for plasma heating and current drive generation (electron Bernstein current drive) at densities where the O and X modes find cutoff values. In the present work, an estimation of the efficiency function of current generated for a relativistic distribution function is presented. The arbitrary large values of the refractive index, due to the EBW propagation properties, have also made necessary the expansion of our calculation up to any Larmor radius order. Particle trapping has been included considering the Okhawa effect, and the

fractions of power absorbed by trapped and circulating particles separately have been estimated. Future work toward implementation of this method to the ray-tracing code used for realistic TJ-II ray trajectories (TRUBA) is also discussed.

KEYWORDS: *electron Bernstein waves, stellarator, current drive*

Note: The figures in this paper are in color only in the electronic version.

I. INTRODUCTION

Not only is current drive generated by electron cyclotron waves an advantage for current sustainment and continuous operation in tokamaks, it also is a good tool for tailoring the rotational transform profile, positioning low-order rationals in the plasma column, modifying the magnetic shear, and thus accessing improved confinement regimes in stellarators.¹⁻⁷ As is well known, the O-modes and X-modes encounter cutoff density values that electron Bernstein waves (EBWs) do not, and therefore, this property makes them key for current drive generation in overdense plasmas. The viability of current drive generation by means of EBW heating [electron Bernstein current drive (EBCD)] in stellarators under this condition has been experimentally demonstrated.⁸ Moreover, the propagation properties and the electrostatic nature of EBWs provide them with arbitrarily large values of both parallel (N_{\parallel}) and perpendicular (N_{\perp}) refractive indexes,⁹ which implies a drastic change in the resonance condition in momentum space and, consequently, widens the integration limits in the parallel momentum for the absorbed power density calculation,

causing electrons with large parallel velocity to resonate. For heating and current drive purposes, an EBW heating system is being installed in the TJ-II stellarator¹⁰ (O-X-B scenario) at first harmonic (28 GHz), 300 kW of power injected, and 100 ms of pulse length.¹¹

The properties of EBW in TJ-II are shown in Ref. 12, including the development of a ray-tracing code based on a weakly relativistic dispersion relation, which is suitable for performing such studies.

The remainder of the paper is organized as follows: Section II shows the efficiency function, Sec. III is devoted to the inclusion of trapped particles both in current drive and power absorption, and Sec. IV presents the conclusions.

II. EFFICIENCY FUNCTION AND CURRENT GENERATED

Our calculation of the current drive efficiency is based on the asymmetric modification of the electron resistivity in momentum space.¹³ Assuming a completely ionized pure hydrogen plasma—thus, the ion charge state $Z_i = 1$ from now on—the fully relativistic efficiency function for a Maxwellian distribution function and any angle of propagation is¹⁴

*E-mail: josemanuel.garcia@ciemat.es

$$\eta(\mathbf{u}) = \frac{\delta J_{\parallel}}{\delta P_d} = G(u) \left[N_{\parallel} - \frac{u_{\parallel}}{u^2} (\gamma + 2) \right] + \frac{2uu_{\parallel}}{\gamma^2}, \quad (1)$$

where $\mathbf{u} = \mathbf{p}/mc$, $\gamma = (1 + \mathbf{u}^2)^{1/2}$ is the Lorentz relativistic factor, and $G(u)$ is expressed as

$$G(u) = 2 \left(\frac{\gamma + 1}{\gamma - 1} \right) \frac{u^2 - 2\gamma \ln \gamma}{\gamma u}. \quad (2)$$

For a review on current drive physics, see Ref. 1, where the equivalence of the method used here and the adjoint one, which is explored in Ref. 15, is established. The induced current density parallel to the magnetic field in terms of the efficiency function can be written as follows¹⁶:

$$J_{\parallel} = A \int d\mathbf{u} \frac{\delta J_{\parallel}}{\delta P_d} \sum_s w_s(\mathbf{u}), \quad \text{with } A = \frac{2\pi\epsilon_0^2 mc^2}{n\Lambda e^3}, \quad (3)$$

where

n = electron density

m = mass

e = electric charge

c = speed of light

Λ = coulomb logarithm

and the sum runs over the harmonic order s . Once the integration of Eq. (3) over u_{\perp} has been carried out, we can rewrite the current density parallel to the magnetic field as

$$J_{\parallel} = A \int du_{\parallel} \eta(u_{\parallel}) \sum_s w_s(u_{\parallel}). \quad (4)$$

The absorbed power density in momentum space w_s at harmonic s takes the following form (see, e.g., Ref. 17):

$$w_s(u_{\parallel}) = \frac{\pi\epsilon_0 \mu^2 \omega_p^2}{4\omega K_2(\mu)} |\mathbf{\Pi}_s \cdot \mathbf{E}|^2 \exp(-\mu\gamma) \times \delta(\gamma - s\omega_c/\omega - N_{\parallel}u_{\parallel}), \quad (5)$$

where

ω_p = electron plasma frequency

ω = wave frequency

$\mu = mc^2/T$

T = electron temperature

K_2 = second-order MacDonald function.

The factor $\delta(\gamma - s\omega_c/\omega - N_{\parallel}u_{\parallel})$ in $w_s(u_{\parallel})$ is due to the absorbed power being different from zero only for resonant electrons. In the polarization term $|\mathbf{\Pi}_s \cdot \mathbf{E}|$, $\mathbf{E} = E\mathbf{e}$ is the wave electric field, and $\mathbf{\Pi}_s$ is expressed as follows:

$$\mathbf{\Pi}_s = \left(\frac{sJ_s(\rho)}{\rho}, -iJ'_s(\rho), J_s(\rho) \frac{u_{\parallel}}{u_{\perp}} \right), \quad (6)$$

where $J_s(\rho)$ are the Bessel functions of the first kind with argument $\rho = N_{\perp}u_{\perp}\omega_c/\omega$. In contrast with previous works that referred to electron cyclotron waves,^{16,17} where Bessel functions in Eq. (6) can be approximated only by the first term, for EBWs with $N_{\perp} \gg 1$, Bessel functions have been expanded iteratively until their convergence. In order to obtain the corresponding N_{\perp} and polarization of the Bernstein wave \mathbf{e} , given the values of N_{\parallel} , wave frequency, and plasma parameters, the dispersion relation for a weakly relativistic Maxwellian distribution function up to the second order in Larmor radius has been solved.^{18,19} This expansion up to a lowest order in Larmor radius than the one used for the absorption density calculation using Eqs. (5) and (6) is sufficient for this purpose since it is used to determine the optical properties of our wave (\mathbf{e} and N_{\perp}), which is equivalent to assuming that it behaves optically as the first Bernstein mode. In this way the distribution function is just an algebraic equation and can be easily solved. On the other hand the power absorption is more sensitive to the number of terms taken into account in Eq. (6) than to the introduction of these first Bernstein mode \mathbf{e} and N_{\perp} . The only quantity left for the calculation, in order to obtain the correct units for the current density J_{\parallel} and absorbed power density w_s , is then the wave electric field amplitude E . This has been approximated by the following relation between the energy density associated with the wave and its electric field: $U \approx [(\omega^2 + \omega_p^2)/2\omega_p^2]^{1/2} \epsilon_0 E^2$ (Ref. 20). This relation assumes that electrons are moving coherently with the wave electric field oscillation, and the aim of its use is to obtain correct units and acceptable orders of magnitude for the current and power densities. On the other hand, the global current efficiency ξ_{CD} does not depend on E , and that is the physical quantity of interest in the case we couple this tool into a ray-tracing code.

The results for the absorption coefficient, considering only the first harmonic ($s = 1$), are shown in Fig. 1 for $N_{\parallel} = 0.4$ and $N_{\parallel} = 1.2$. It can be seen that the difference between the expansion up to the first relevant order and the convergent one becomes larger in the vicinity of the resonance frequency $\omega = 28$ GHz. That difference is of the same order of magnitude in both cases, due to the similar values of N_{\perp} that satisfy the dispersion relation for both parallel refractive index values. Apart from this fact the only remarkable difference lies on the frequency interval with nonzero absorption coefficient, larger for $N_{\parallel} = 1.2$.

With the total absorbed power density P_s , performing the integration of w_s over the parallel momentum of

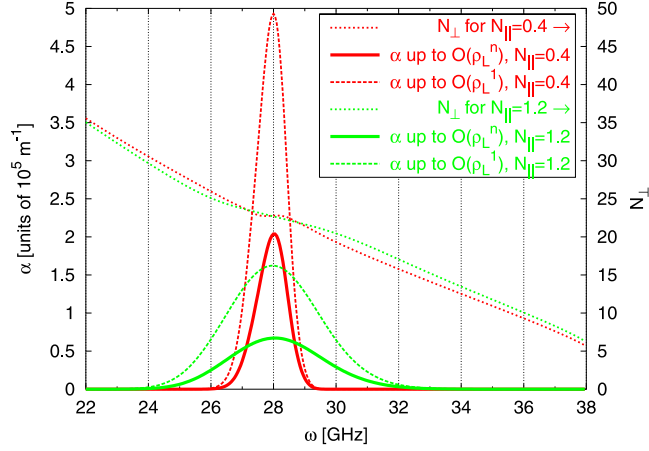


Fig. 1. Comparison of the absorption coefficient as a function of the wave frequency ω up to the lowest relevant order in Larmor radius (dashed thin lines), and for an expansion up to the convergent order (continuous thick lines), for $N_{\parallel} = 0.4$ and $N_{\parallel} = 1.2$, with $T_e = 1$ keV, $n_e = 1 \times 10^{19} \text{ m}^{-3}$, and $B = 1$ T. The dotted lines are referred to the right y-axis and represent the corresponding values of N_{\perp} that satisfy the dispersion relation for Bernstein mode at first harmonic (28 GHz).

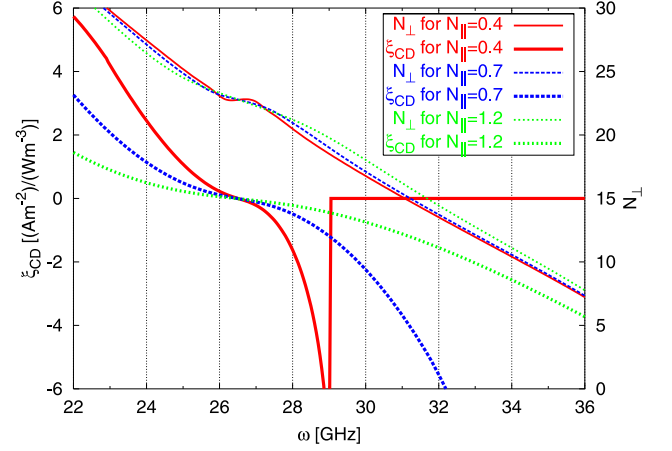


Fig. 2. Dependence of the efficiency function ξ_{CD} on the wave frequency ω (thick lines), for $N_{\parallel} = 0.4$, $N_{\parallel} = 0.7$, and $N_{\parallel} = 1.2$, and their corresponding curves of N_{\perp} satisfying the dispersion relation for Bernstein mode at first harmonic (thin lines). Plasma parameters: $T_e = 1$ keV, $n_e = 1 \times 10^{19} \text{ m}^{-3}$, and $B = 0.95$ T.

the resonant electrons, the macroscopic current drive efficiency ξ_{CD} is finally given as

$$\xi_{CD} = \frac{J_{\parallel}}{P_s} = \frac{\int \eta(v_{\parallel}) w_s(v_{\parallel}) dv_{\parallel}}{\int w_s(v_{\parallel}) dv_{\parallel}}. \quad (7)$$

As is shown in Fig. 2 the current efficiency $\xi_{CD}(\mathbf{r})$ decreases as N_{\parallel} increases and becomes flatter for $N_{\parallel} \geq 1$. It is also seen that the frequency interval where the efficiency is different from zero is wider for the latter case. This is shown also in Fig. 3, where the induced parallel current density decreases remarkably as N_{\parallel} becomes larger, although the driven current takes place in a wider frequency range because the resonance condition is satisfied in this wider frequency interval. The conclusion that can be drawn from these features is that the advantage that Bernstein waves represent for the current generation in a wider range in parameter space, due to its capability to reach a high parallel component of the refractive index along the ray trajectories, counteracts with the fall in the current efficiency as the N_{\parallel} increases.

III. PARTICLE TRAPPING EFFECTS

It is well known that particles with momentum \mathbf{u} are trapped if

$$(u_{\parallel}/u) \leq \mu_t \equiv (1 - B/B_{\max})^{1/2}, \quad (8)$$

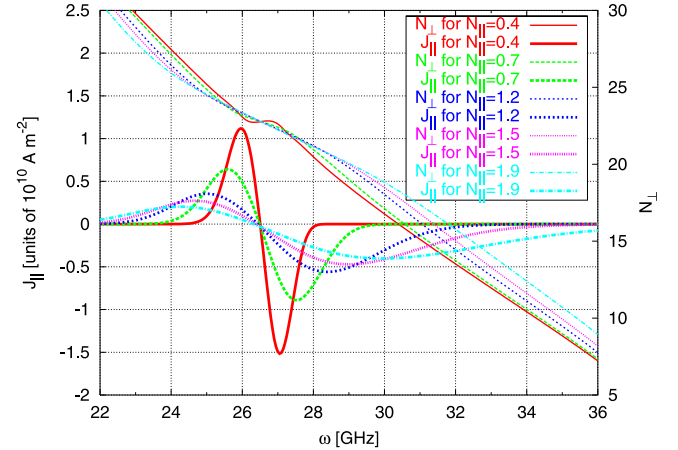


Fig. 3. Induced parallel current density J_{\parallel} as a function of the wave frequency ω , for several values of N_{\parallel} (thick lines) and their corresponding N_{\perp} obeying the dispersion relation for Bernstein mode at first harmonic (thin lines). As before, $T_e = 1$ keV, $n_e = 1 \times 10^{19} \text{ m}^{-3}$, $B = 0.95$ T, and 300 kW of injected power.

where

μ_t = trapping parameter

B = local magnetic field

B_{\max} = maximum magnetic field on a field line, or approximately, on the magnetic surface, since a magnetic field line is dense in a magnetic surface for nonrational rotational transform values.

The cone defined by the equality in Eq. (8) cuts the resonance condition curve into two points in momentum space:

$$u_{1,2} = \frac{Y_s N_{\parallel} \mu_t^2 \pm \mu_t (Y_s^2 - 1 + \mu_t^2 N_{\parallel}^2)^{1/2}}{1 - \mu_t^2 N_{\parallel}^2}, \quad (9)$$

where $Y_s = s\omega_c/\omega$. These intersections fix the integration limits for the parallel current calculation in Eq. (7), in order to exclude trapped particles from the net current contribution. At the same time, this procedure applied to the integration of $w_s(u_{\parallel})$ provides a useful and easy way to distinguish between the contribution to absorption due to trapped and circulating particles separately.²¹ This approach to the effect of trapped electrons on current generation, together with the diffusion of circulating electrons into the trapping region in momentum space, which is explained below, might overestimate the result of current drive because the slowing-down equations governing the present model do not take into account the change in the slowing-down frequency due to the presence of a large population of trapped electrons in the trajectory of those that produce current. Integration of the Langevin equations considering two different slowing-down frequencies could be a task for future work. For a better knowledge of the trapped electrons on current drive using the adjoint formalism, see Refs. 22, 23, and 24.

For the calculations presented in Figs. 4 through 8, a set of profiles similar to those measured in TJ-II has been considered. The magnetic field and trapping parameter profiles have been taken as $B \approx B_0 r_0 / (r_0 + ar_{eff})$ and

$\mu_t \approx 0.08 + 0.27|r_{eff}|$, where $r_{eff} = r/a$ is the normalized radius, r is the radial coordinate, $a = 0.2$ m is the mean minor radius of the plasma, and $r_0 = 1.5$ m is the major radius of the device. Note that the latter expression for the trapping parameter and the magnetic field profile do

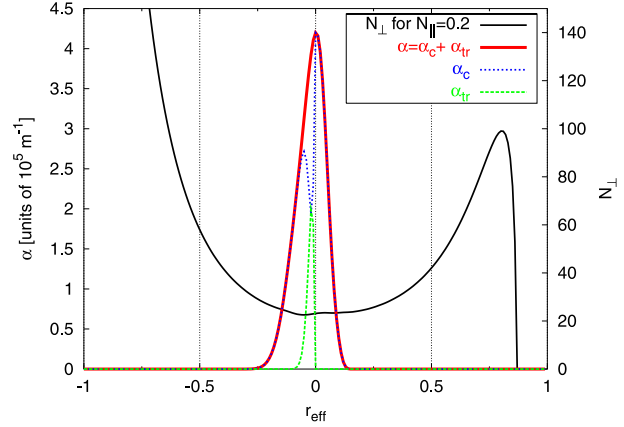


Fig. 5. Comparison of the absorption coefficient for $N_{\parallel} = 0.2$ as a function of the effective radius r_{eff} , considering all the resonant electrons in momentum space α (thick continuous line), circulating electrons α_c (dotted line), and trapped electrons α_{tr} (dashed line), in a plasma with electron density and temperature at the core $n_{e0} = 1 \times 10^{19} \text{ m}^{-3}$ and $T_{e0} = 1 \text{ keV}$, respectively. TJ-II typical profiles for magnetic field and ripple have been considered. The thin continuous line represents the N_{\perp} obeying the dispersion relation for Bernstein mode at first harmonic.

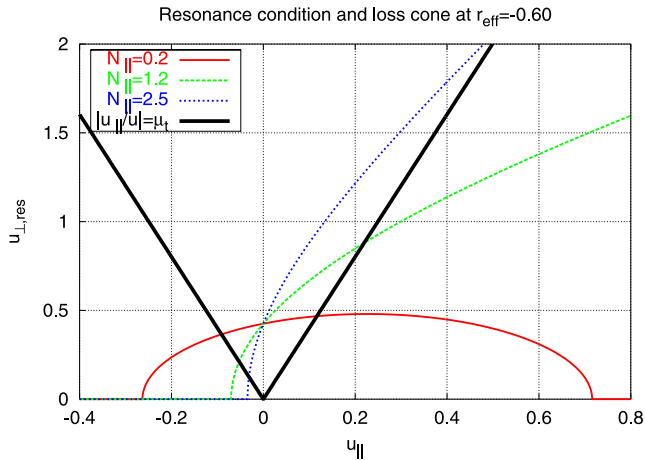


Fig. 4. Resonance condition for $N_{\parallel} = 0.2$, $N_{\parallel} = 1.2$, and $N_{\parallel} = 2.5$, at the radial position $r_{eff} = -0.60$, in a plasma with similar parameters and profiles as the one confined in TJ-II. Electron density and temperature at the core $n_{e0} = 1 \times 10^{19} \text{ m}^{-3}$ and $T_{e0} = 1 \text{ keV}$, $B(r_{eff} = -0.60) \approx 1.1 \text{ T}$ and $\mu_t(r_{eff} = -0.60) \approx 0.24$. The solid thick line is the limit over which resonant electrons become trapped ($\mu_t = u_{\parallel}/u$).

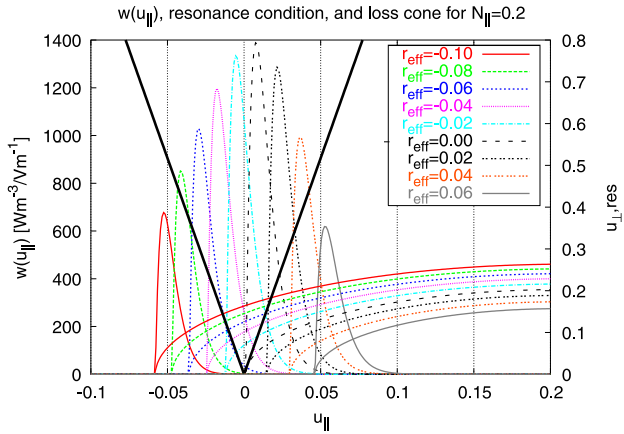


Fig. 6. In the left y-axis: absorbed power density in momentum space $w(u_{\parallel})$ for a unitary wave electric field at different radial positions and the same $N_{\parallel} = 0.2$, as in Fig. 5. In the right y-axis: perpendicular momentum $u_{\perp,res}$ obeying the elliptical resonance condition at those radial positions, together with the trapping cone at the last position (continuous thick line). Same plasma parameters and profiles as Fig. 5.

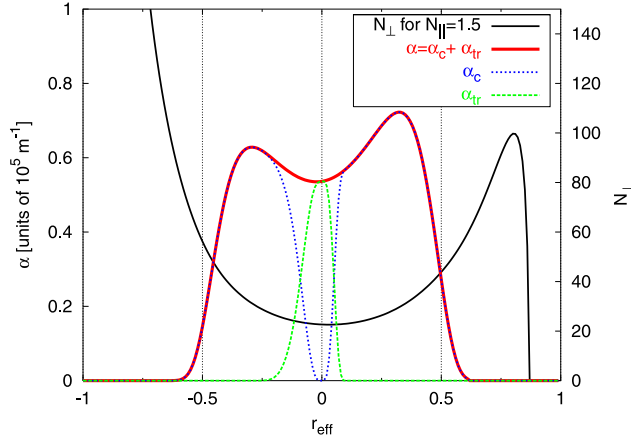


Fig. 7. Comparison of the absorption coefficient, for $N_{\parallel} = 1.5$ as a function of the effective radius r_{eff} , considering all the resonant electrons in momentum space α (thick continuous line), circulating electrons α_c (dotted line), and trapped electrons α_{tr} (dashed line), in a plasma with electron density and temperature at the core $n_{e0} = 1 \times 10^{19} \text{ m}^{-3}$ and $T_{e0} = 1 \text{ keV}$, respectively. TJ-II typical profiles for magnetic field and ripple have been considered. The thin continuous line represents the N_{\perp} obeying the dispersion relation for Bernstein mode at first harmonic.

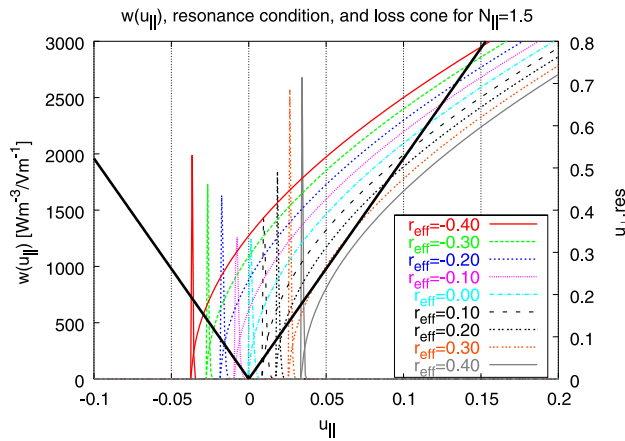


Fig. 8. In the left y-axis: absorbed power density in momentum space $w(u_{\parallel})$ for a unitary wave electric field at different radial positions and the same $N_{\parallel} = 1.5$ as in Fig. 7. In the right y-axis: perpendicular momentum $u_{\perp, \text{res}}$ obeying the hyperbolic resonance condition at that radial position, together with the trapping cone at the last position (continuous thick line). Same plasma parameters and profiles as Figs. 5 through 8.

not conflict with Eq. (8) since as has already been mentioned above, the value of B_{max} is referred to as the maximum value of the magnetic field on a given magnetic surface, and not on the magnetic field radial profile, and

thus, μ_t shows a dependence on r_{eff} that in TJ-II can be fitted as the expression written above. The density and temperature profiles adopted have been taken as $T_e = T_{e0} \exp[-(r/0.08)^2]$ and $n_e = n_{e0}[1 - (r/a)^4]^2$. The symmetry of a circular tokamak has also been considered, where our normalized radius range represents its equatorial plane.

The trapped particle cone and the resonance curve for different values of $|N_{\parallel}|$, larger and smaller than 1, which separates the case where the resonance condition is an ellipse from the case where it is a hyperbola, can be seen in Fig. 4. This change in the resonance condition can be clearly seen as the parallel refractive index increases. A plasma with the profiles written above, with $T_{e0} = 1 \text{ keV}$ and $n_{e0} = 1 \times 10^{19} \text{ m}^{-3}$, at $r_{\text{eff}} = -0.6$ has been considered. In that radial position, a significant difference in the width of the interval where the resonance condition is above the trapping limit ($u_{\parallel}/u = \mu_t$) can be observed for the different values of N_{\parallel} taken. This means that a very variable population of resonant trapped particles is found. This fact is even more evident in the case in which $|N_{\parallel}| > 1$. For example, for $N_{\parallel} = 2.5$ nearly the whole right arm of the hyperbola is over that limit, and thus, the population of resonant trapped electrons is far larger than in the other two cases, where a small interval of the resonant electrons in momentum space is trapped.

As has been stated above, the contribution of the trapped electrons to the total absorbed power density can be estimated, just modifying the integration limits for the calculation of $P_s(\mathbf{r})$, in order to exclude those electrons present in the trapping region in momentum space. The total absorbed power is given by the integration of Eq. (5): $P_s = \int w_s(u_{\parallel}) du_{\parallel}$. The absorbed power by trapped particles is given by $P_{s, \text{trapped}} = \sum_i \int_{C_i} w_s(u_{\parallel}) du_{\parallel}$, where C_i are the domains of integration in parallel momentum u_{\parallel} where the resonance curve is over the trapped particle cone. This calculation is relevant for estimating the behavior of particles that absorb the power and the enhancement of pumpout (see Ref. 25). The change of scenario in the resonance condition from an elliptically shaped curve ($|N_{\parallel}| < 1$) to a hyperbolic one ($|N_{\parallel}| > 1$) also makes it necessary to define cutoff values for the integral limits as these tend to $\pm\infty$ in order to perform a numerical calculation of Eq. (7), and taking into account that the population of electrons beyond those limits is negligible. The absorption coefficient α is related to the absorbed power density P_s as $\alpha(\mathbf{r}) = P_s(\mathbf{r}) \pi b^2$, where b is the beam radius, and which has been considered 2 cm in our calculations.

Figure 5 shows the absorption coefficient α as a function of r_{eff} for $N_{\parallel} = 0.2$ (elliptical resonance condition), considering the already mentioned profiles. The absorption coefficient, taking into account the whole population of resonant electrons for the Bernstein mode of propagation at first harmonic (28 GHz), is represented in comparison with the absorption coefficient due to the trapped population α_{tr} and the circulating one α_c . In this case it is

shown that the fraction of the power absorbed by trapped particles is smaller than the one absorbed by passing ones for all r_{eff} , but it is far from being negligible close to $r_{eff} = 0$. This contribution of trapped particles to the absorbed power where the ripple of the device is lower and the trapped particle cone is narrower can be explained with the shape of the resonance condition in relation to the trapping cone and the absorbed power density in momentum space. This can be observed in Fig. 6, for negative values of the normalized radius in the vicinity of the center of the plasma ($r_{eff} = -0.02$), where Fig. 5 shows the maximum contribution of trapped particles to the absorption coefficient, and the absorbed power density in momentum space $w_s(u_{||})$ shows a peaked profile centered between the cuts of its corresponding resonance curve and the trapping cone. In order to avoid unnecessary confusion to the figure, only the trapping cone for the last of the values of r_{eff} has been represented in Figs. 6 and 8 since its angle does not change noticeably along the interval.

The absorption coefficient α for $N_{||} = 1.5$ (hyperbolic resonance condition) in Fig. 7 is also shown for the Bernstein mode at first harmonic (28 GHz). It is seen that the width of the nonzero absorption coefficient region is larger than in the former case. It can be observed that the contribution to the absorption coefficient by trapped particles becomes the only one to the total absorption coefficient in the center. Figure 8 shows, for $r_{eff} = 0$ and $N_{||} = 1.5$, the absorbed power density profile in momentum space whose main contribution lies between the intersections of the right arm of the hyperbolic resonance condition and the trapping cone. This explains why such an important contribution to the absorption coefficient of trapped electrons takes place in the center, as Fig. 7 shows.

In addition, the diffusion in momentum space can produce that circulating particles become trapped, which is known as the Ohkawa effect,²⁶ and thus, the efficiency function takes the following form¹⁶:

$$\begin{aligned} \eta_T(\mathbf{u}) &= \eta(\mathbf{u}) - \frac{u_{||}}{|u_{||}|} \frac{1 + 2g(\mathbf{u})}{[1 - g(\mathbf{u})]^2 \sqrt{g(\mathbf{u})}} \left(\frac{\mu_t u}{|u_{||}|} \right) \\ &\times \frac{\partial \chi(\mathbf{u}_T)}{\partial u_T} \left(\frac{\gamma - 1}{\gamma + 1} \right) \\ &\times \frac{1}{u^2} \left\{ 2 + Y_s - u_{||} N_{||} \left(\frac{u_{\perp}}{u_{||}} \right)^2 \right\}, \end{aligned} \quad (10)$$

where $\chi_T(\mathbf{u}) = \chi_T(\mathbf{u}) - \chi(\mathbf{u}_T)$ is the modified response function. Being the response function the total contribution of a single particle to the current

$$\chi(\mathbf{u}) = -\frac{ec}{\gamma} \int_0^{\infty} u_{||}(t, \mathbf{u}) dt, \quad (11)$$

and \mathbf{u}_T is the momentum at which a circulating particle becomes trapped, with the module and parallel component given by

$$u_{T,||} = \frac{u_{||}}{|u_{||}|} \mu_t u_T \quad \text{and} \quad u_T = \frac{2\sqrt{g(\mathbf{u})}}{1 - g(\mathbf{u})} \quad (12)$$

with

$$g(\mathbf{u}) = \left(\frac{\mu_t u}{|u_{||}|} \right) \frac{\gamma - 1}{\gamma + 1}, \quad (13)$$

and the derivative of the response function that appears in Eq. (10) is calculated as follows

$$\frac{\partial \chi(u_T)}{\partial u_T} = \mu_t \left[2 \left(\frac{u_T}{\gamma_T} \right) - \frac{2}{\gamma_T} G(u_T) \right]. \quad (14)$$

The results of parallel current density as a function of the frequency, considering the efficiency as in Eq. (10), are shown in Figs. 9 and 10. As can be seen in Fig. 9, for constant parallel refractive index $N_{||} = 1$ and different values of μ_t , the sign of the current can be changed because of the effect of particle trapping. A frequency range of flat and null current grows with μ_t as well, which shows a deterioration in current production. Furthermore, the changes of the current sign are more stressed in the case when the maximum of the current is larger, as Fig. 10 shows for $N_{||} = 0.4$. In Figs. 9 and 10, the peaks with maximum absolute value of current $J_{||}$ are moving away from each other as μ_t and $N_{||}$ increase, with the dependence of this fact being stronger on the latter parameter.

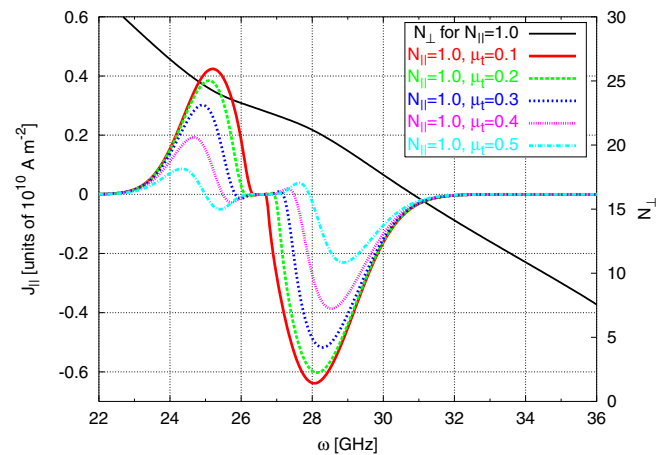


Fig. 9. Parallel current density dependence on the wave frequency for fixed values of $N_{||} = 1$, and varying μ_t , for $T_e = 1$ keV, $n_e = 1 \times 10^{19} \text{ m}^{-3}$, and $B = 0.95$ T. On the right y-axis the values of N_{\perp} that satisfy the dispersion relation for Bernstein mode at first harmonic.

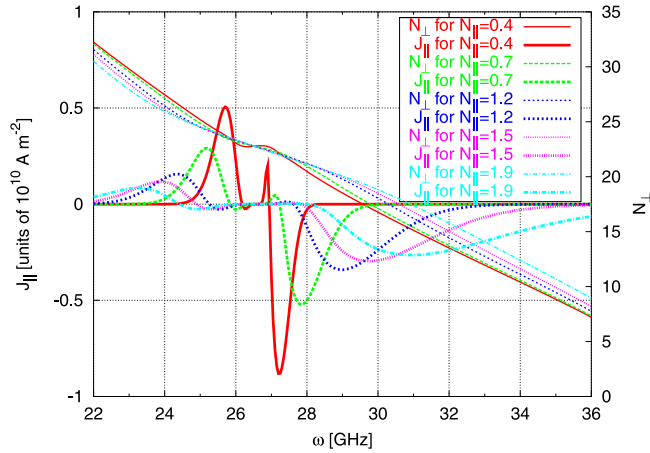


Fig. 10. Parallel current density dependence on the wave frequency (thick lines) for fixed values of $\mu_t = 0.4$, and varying $N_{||} = 1$, for $T_e = 1$ keV, $n_e = 1 \times 10^{19} \text{ m}^{-3}$, and $B = 0.95$ T. On the right y-axis the values of $N_{||}$ that satisfy the dispersion relation for Bernstein mode at first harmonic (thin lines).

Finally, Fig. 11 shows the integration of $J_{||}$ along the equatorial line of a circular tokamak cross section, in order to obtain the total parallel current generated $I_{||}$ as a function of the parallel refractive index in a typical TJ-II plasma. Although this integration path would not be a real ray trajectory, some conclusion can be drawn from this approach. The same profiles as those described above

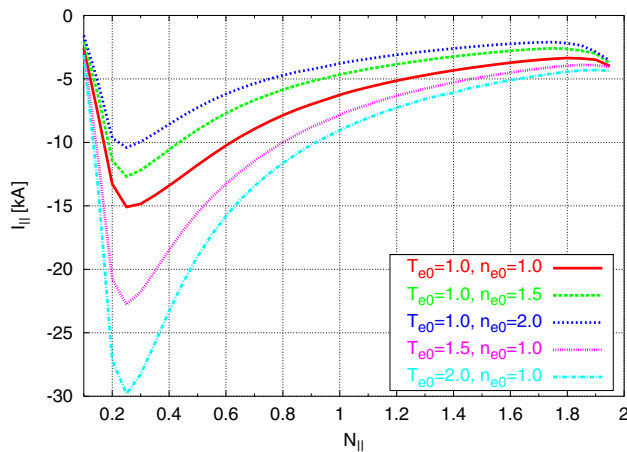


Fig. 11. Total parallel current $I_{||}$ dependence on $N_{||}$ obtained integrating $J_{||}$ along a ray trajectory crossing a plasma along its equatorial plane for different values of density and temperature at the core and the profiles already mentioned in the text. Temperatures in kilo-electron-volts and density in units of 10^{19} m^{-3} .

for Figs. 4 through 8 have been considered for the magnetic field, trapping parameter, electron density, and temperature, varying the central values of these last two parameters. Figure 11 also shows the existence of an optimal value of $N_{||}$ for current generation, typically around $N_{||} \approx 0.2$, as well as a growth of the current with the temperature, which comes from the fall of collisionality with it, in contrast with the opposite behavior with the density.

IV. CONCLUSIONS

An estimate of the EBCD has been calculated for arbitrary values of $N_{||}$ and trapping parameter μ_t , assuming a TJ-II-like circular tokamak. The results show a dependence of current efficiency and current density on both parameters, stronger on the first of them. A larger value of $N_{||}$ causes a broadening of absorption in frequency, or equivalently in magnetic field values at a fixed frequency, and thus, current generation at any position along the beam trajectory takes place more easily. In contrast, the efficiency and current density decrease from an optimal parallel refractive index on. More detailed work on exploring the advantage that can be taken from the existence of this optimal parallel refractive index value is of interest since after conversion has taken place, the ray trajectories of the Bernstein wave are highly unpredictable, and for that reason the benefit becomes difficult to exploit. It is left as an immediate task the implementation of this tool into the ray-tracing code TRUBA, currently in use in TJ-II, for a deeper understanding under real ray paths and operational conditions in a complex stellarator. More accurate results than those presented here are expected to be obtained, since the absorbed power density is calculated by the code, and the only quantity needed for the current drive calculation will be the global efficiency ξ_{CD} , which does not require any estimation of the electric field modulus since it does not depend on it. Another task could be the comparison between the current density provided by the TRUBA code²⁷ and that using Eq. (5). The estimation of the electric field amplitude needed for the latter method could be solved using the antihermitic part of the dielectric tensor, calculated by the ray-tracing code, and the application of its relation with the wave energy density U and its electric field amplitude E for Bernstein waves.²⁸ Also of interest for future work concerning pumpout studies is the method here used to quantify the contribution of trapped particles on the total absorbed power, changing the integral limits of $w_s(u_{||})$. This shows how the relative positions of the resonance condition, trapping cone, and absorbed power density in momentum space play a decisive role in the trapped particle contribution, despite the fact that we look into a zone with low ripple.

REFERENCES

1. N. J. FISCH, *Rev. Mod. Phys.*, **59**, 175 (1987).
2. V. ERCKMANN and U. GASPARINO, *Plasma Phys. Control. Fusion*, **36**, 1869 (1994).
3. ITER PHYSICS EXPERT GROUP ON ENERGETIC PARTICLES, HEATING, AND CURRENT DRIVE and ITER PHYSICS BASIS EDITORS, *Nucl. Fusion*, **40**, 1429 (2000).
4. R. PRATER, *Phys. Plasmas*, **11**, 2349 (2004).
5. F. CASTEJÓN et al., *Plasma Phys. Control. Fusion*, **47**, B53 (2005).
6. V. I. VARGAS et al., *Nucl. Fusion*, **47**, 1367 (2007).
7. D. LÓPEZ-BRUNA et al., *Europhys. Lett.*, **82**, 65002 (2008).
8. H. LAQUA et al., *Nucl. Fusion*, **43**, 1324 (2003).
9. H. P. LAQUA, *Plasma Phys. Control. Fusion*, **41**, R1 (2007).
10. C. ALEJALDRE et al., *Fusion Technol.*, **17**, 131 (1990).
11. A. FERNÁNDEZ et al., *Fusion Eng. Des.*, **74**, 325 (2005).
12. F. CASTEJÓN et al., *Nucl. Fusion*, **48**, 075011 (2008).
13. N. J. FISCH and A. H. BOOZER, *Phys. Rev. Lett.*, **45**, 720 (1980).
14. N. J. FISCH, *Phys. Rev. A*, **24**, 3245 (1980).
15. V. ERCKMANN et al., *Plasma Phys. Control. Fusion*, **34**, 1917 (1992).
16. F. CASTEJÓN et al., *Phys. Fluids B*, **4**, 3689 (1992).
17. I. FIDONE et al., *Phys. Fluids A*, **31**, 2300 (1988).
18. M. BORNATICI et al., *Nucl. Fusion*, **23**, 1153 (1983).
19. C. ALEJALDRE and F. CASTEJÓN, *Phys. Fluids B*, **1**, 2201 (1989).
20. K. T. McDONALD, <http://arXiv.org/abs/physics/0312025v1> (2003).
21. V. ERCKMANN et al., *Fusion Sci. Technol.*, **52**, 291 (2006).
22. R. N. COHEN, *Phys. Fluids*, **30**, 2442 (1980).
23. M. TAGUCHI, *Plasma Phys. Control. Fusion*, **31**, 241 (1989).
24. Y. R. LIN-LIU et al., *Phys. Plasmas*, **10**, 4064 (2003).
25. F. CASTEJÓN et al., *Phys. Plasmas*, **15**, 012504 (2008).
26. T. OHKAWA, GA-A13847, General Atomics, National Technical Information Service Document PB2000-108008. (1976).
27. F. CASTEJÓN et al., *Fusion Technol.*, **52**, 230 (2006).
28. J. DECKER and A. K. RAM, *Phys. Plasmas*, **13**, 112503 (2006).